CrystEngComm

Dynamic Article Links ▶

HIGHLIGHT

Surface transmission electron diffraction for SrTiO₃ surfaces

Danielle M. Kienzle[a] and Laurence D. Marks[b]

This work highlights transmission electron diffraction (TED) for determining surface structures and understanding the model perovskite system, SrTiO₃, which has been extensively studied due to its wide array of applications and simple bulk structure. TED is a powerful tool for surface science and has been the key to determining several SrTiO₃ surface reconstructions.

1. Introduction

The surface is where the action is. It is the boundary between the bulk of a material and its environment whether it is air, water, or another material. How a surface interacts with its environment will ultimately affect its properties. Knowledge of how a surface interacts is paramount to many technologies and industrial processes such as heterogeneous catalysis, one of the workhorses of the chemical industry. Reactants interact with a catalyst by adsorbing onto its surface, forming chemical bonds with surface atoms, which allows for a reaction to proceed efficiently. But, with which specific atoms do reactants bond? Is the local bonding of one surface atom preferable to another? Knowing the specific atomic sites that are active in a catalytic reaction would not only help us understand the process more completely, but would also enable us to design better catalysts. This is just one example of how a comprehensive knowledge of a material's surface structure could open doors to technological advancements.

SrTiO₃ is one of the most commonly investigated oxide for surface studies because of its simple perovskite structure and its usefulness for a broad range of applications including epitaxial thin film growth of high-T_c superconductors[1–3] because of the ability to obtain atomically flat SrTiO₃ surfaces.[4,5] It has also proven itself useful as an interface layer (or buffer layer) in electronic devices such as between GaAs and silicon[6,7] or as a gate dielectric in metal-oxide semiconductor based structures.[8,9] It may also be possible to take advantage of unique surface nanostructures that SrTiO₃ can exhibit, such as nanolines[10] or arrays of nanodots[11] for use as nanowires or quantum dots. More recently, SrTiO₃ has garnered further interest due to the unique electronic properties observed such as a conductive 2D-electron gas formed at a UHV-cleaved SrTiO₃ surface[12] or similarly at SrTiO₃/LaAlO₃ interfaces.[13]

For all these applications, it is very important to know the surface morphology as well as to understand how and why it forms. There is quite a large amount of literature already devoted to this topic. It is especially interesting for surface studies because of the many surface reconstructions that have been observed, including a series of $n \times n$ reconstructions on the (111) surface,[14] $n \times 1$ and $1 \times n$ reconstructions on the (110) surface[15,16] and an even larger number for the (001). Table 1 is a compilation of reported reconstructions that have been experimentally observed on the SrTiO₃ (001) surface as well as the sample treatment and detection technique.

There are thousands of known bulk crystal structures along with a thoroughly developed set of analogies and rules to help characterize the bulk structure of an unknown material. The same cannot be said for the atomic surface structure, which may deviate from the bulk. When the "surface" of a material is discussed, it refers to the layer of atoms where the repetition of the bulk ends. These atoms do not have the same local bonding environment as the atoms in the bulk and are left under-coordinated with "dangling bonds." In most cases, the arrangement of atoms at the surface can achieve a lower energy by structural relaxation or reordering. The arrangement of surface atoms can often be drastically different, as observed with SrTiO₃, leading to different properties. If the surface atoms are arranged with a periodically repeating unit larger than that of the bulk, the resulting structure is referred to as a surface reconstruction and is named by its surface unit cell size relative to that of the bulk's. An example of this is shown in Fig. 1 comparing the bulk surface unit cell with the known SrTiO₃ (001) 2 × 1 reconstructed surface unit cell.

Taking the case of the perovskite SrTiO₃ along its [001] direction, the bulk structure can be described as alternating layers of SrO and TiO₂. Truncating the

[a]Northwestern University, 2220 Campus Drive, Evanston, IL, USA.
E-mail: d-kienzle@u.northwestern.edu;
Fax: 847-491-7820; Tel: 847-491-7809
[b]Northwestern University, 2220 Campus Drive, Evanston, IL, USA.
E-mail: l-marks@northwestern.edu;
Fax: 847-491-7820; Tel: 847-491-7809

Table 1 Observed surface reconstructions of the $SrTiO_3$ (001) surface

Reconstruction	Sample Prep.	T/K	Atmosphere	Time (min.)	Technique
(1 × 1)	Sputtered	1100	UHV	60	LEED[26]
	Sputtered	900	10^{-6} mbar O_2		LEED[27]
	Sputtered	1200	UHV	few min.	LEED[28]
		873	UHV	10–120	LEED[2]
	e^- bombardment			60	LEED[29]
		973	10^{-4} mbar O_2	60	LEED[30]
	BHF etch	873	UHV	30	LEED+STM[11]
(2 × 1)	Sputtered	1100	10^{-5} mbar O_2		LEED[26]
	followed by:		UHV	15	
		1023–1073	HV	60	RHEED[31]
		1073	UHV	20–120	LEED[2]
	Etched	873–1073	UHV	30	LEED+STM[32]
	BHF etch	1173	10^{-2} mbar O_2	30min	STM+RHEED[33]
	Sputtered	1223–1323	flowing O_2	120–300	HREM+TED[20]
(2 × 2)	Sputtered	1100	10^{-5} mbar O_2		LEED[26]
	followed by:	900	UHV	15	
		1173–1223	HV	30–120	LEED[2]
		1473	UHV		STM[34]
		<973	10^{-10} mbar O_2	several hrs.	LEED[30]
	Etched	1273	UHV	20	STM[35]
c(4 × 2)	(2 × 1) + sputtering	1133	UHV	5	STM[11]
	Sputtered	1173–1673	UHV	15	LEED+STM[32]
	Sputtered	1123–1203	flowing O_2	120–300	HREM+TED[21]
	mechano-chemically polished	1100C	flowing O_2		LEED+STM[36]
	followed by:	950C	5×10^{-7}–5×10^{-5} mbar H_2	120min	
c(4 × 4)	(2 × 1)	1173–1673	UHV	30	LEED+STM[32]
	Etched	1273	UHV	20	STM[35]
(4 × 4)	c(4 × 4)	1423	UHV	several secs.	STM[35]
c(6 × 2)		1073–1373	flowing O_2	900	RHEED[31]
	Sputtered	1323–1373	flowing O_2	120–200	HREM+TED[22]
		1373	O_2	several hrs.	LEED[3]
	followed by:	1203	O_2	brief time	
		1223–1373	O_2	240–300	LEED+STM[37]
	followed by:	1223	UHV	120	
	BHF etch	1223	10^{-2} mbar O_2	30min	STM+RHEED[33]
(6 × 2)	(2 × 1)+sputtering	1248	UHV	10	STM[11]
($\sqrt{5} \times \sqrt{5}$)R26.6°	(4 × 4)	1453–1473	UHV	several secs.	STM[35]
		1473	UHV	2	STM[38]
	Etched	1273	UHV	several secs.	STM+AFM[39]
		1073	UHV	30	STM[40]
		1458	UHV	2	
		1103	UHV	120	LEED[41]
($\sqrt{13} \times \sqrt{13}$)R33.7°		1073–1373	flowing O_2	900	RHEED[31]
	($\sqrt{5} \times \sqrt{5}$)R26.6°	1523	UHV	several secs.	STM[35]
	Sputtered + etched	1323	flowing O_2	300	TED[23]
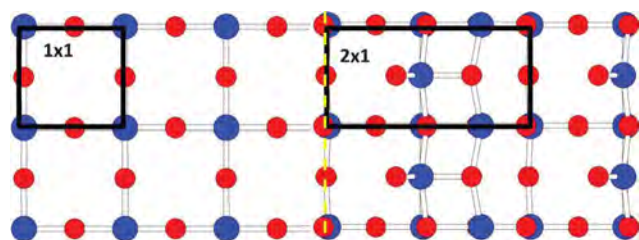
Fig. 1 Top view of $SrTiO_3$ (001) with bulk TiO_2 termination (*left of dashed line*) with 1 × 1 surface unit cell outlined. (*Right of dashed line*) shows the 2 × 1 surface reconstruction[20] with the surface unit cell outlined. The size and periodicity is defined relative to the surface unit cell with the 2 × 1 twice as large in one direction.

bulk will create either a SrO or TiO_2 surface layer depending on where the truncation occurs. As will be later described, these bulk-truncated surface layers are typically not the lowest energy configuration and upon annealing will reconstruct. Along the [110] direction, alternating layers of $SrTiO^{4+}$ and O_2^{4-} make up the bulk and render the surface polar, meaning it will not be valence-neutral and there will be a nominal 2+/2− valence excess, depending on the terminating bulk layer. This is also energetically unfavorable, creating holes in the valence band or electrons in the conduction band.

2. Experimental techniques

2.1 Electron diffraction

From Table 1 it is apparent that low energy electron diffraction (LEED) is the most popular electron probe method for characterizing a surface structure. LEED makes use of an electron beam with a lower energy (20–200 eV) relative to transmission electron diffraction (TED) (100–300 kV). The electrons bombard the sample and are back-scattered forming a

diffraction pattern. Because of the low energy, the electrons have a small mean free path and therefore a shallow sampling depth of a few Angstroms, making LEED a highly surface-sensitive technique. Qualitatively, from a diffraction pattern one can immediately assess the symmetry of the surface structure and the size of the surface unit cell if it differs from that of the bulk, but not the actual position of atoms on the surface. The same is true for a TED pattern.

In a diffraction experiment the intensity of each diffracted beam, related to the square of its wave's amplitude, can be recorded, but the phase cannot. This is what is known as the "phase problem". If the phase and amplitude were known, an inverse Fourier transform would return the real-space structure. Since this is not the case, the phases need to be approximated. This is where the crucial difference between LEED and TED comes in. LEED has more multiple scattering events that make a quantitative analysis much more complicated. A simpler kinematical approximation assumes single scattering events and this is more true for TED.[17] In TED, electrons at a higher energy are transmitted through a thin sample and diffracted by the crystal to form the diffraction pattern. More details on TED are given below.

Transmission electron microscopy (TEM) also has the added benefit of being able to image the exact area of the sample from which a diffraction pattern corresponds. It is simple to qualitatively gauge the state of the surface before recording diffraction patterns. Well-ordered surfaces can exhibit quantized changes in thickness contrast showing steps or facets while a disordered surface may exhibit bend contours signaling stresses within the crystal. An example of this is shown in Fig. 2, where a $SrTiO_3$ (001) sample is imaged before and after being annealed. The annealed sample's surface has reconstructed to a ($\sqrt{13} \times \sqrt{13}$)R33.7° reconstruction ("RT13") and now shows steps with large flat areas and step edges that run perpendicular to one another.

The first step in obtaining good diffraction data is to prepare a very thin TEM sample. For the purposes of surface studies, it is easier to use a single crystal with the specific orientation of interest rather than particles which require more work at the microscope to find and tilt to the desired orientation. Self-supported TEM samples are made by cutting a three millimeter disc from the material and mechanically thinning to roughly 100 microns. A spinning wheel used with diamond slurry is later placed in contact with a rotating sample to thin the center while leaving the edges of the disc sufficiently thick for handling, thus creating a "dimple". The final stage of preparation is yet another thinning stage, this time with a focused beam of Argon ions (2–6eV) bombarding the surface until a small hole is made in the center of the sample. The area surrounding this hole should be sufficiently thin for electrons to transmit through (<200 nm).

There are drawbacks that arise from this method of sample preparation. During the process much damage is inflicted on the sample, including embedded argon ions and an overall reduced and disordered surface; however, this can be overcome by annealing. Again, Fig. 2 shows a TEM image of an as-prepared sample showing signs of stress, dislocations and voids (on left.) After annealing at 700 °C for 3 h (not shown), this stress is no longer present and the sample surface will become uniform and relatively flat. With further annealing at a higher temperature (1050 °C), surface reconstructions form indicated by flat terraces and faceting (on right.) It can be hard to determine the correct annealing temperature and time as it varies for different materials, but in general, there needs to be enough added thermal energy to facilitate surface diffusion. Higher temperatures that enable bulk diffusion will lead to coarsening making thin areas thicker and less ideal for TEM. For the case of $SrTiO_3$, temperatures in the range of 600–800 °C for several hours will allow enough surface diffusion to recover the bulk order and oxidize the surface.. Temperatures in the range of 1000–1200 °C for several hours will allow for surface reconstructions as surface atoms can diffuse to an even lower energy configuration.

When recording a TED pattern, a better signal from the surface can be gained by slightly tilting away from the zone axis. This will attenuate the intensity of the bulk spots to a greater extent than surface spots, thereby increasing the signal-to-noise ratio. Fig. 3 shows a diffraction pattern from a $SrTiO_3$ (001) sample with a RT13 reconstruction. The 1×1 cell corresponding to the bulk is outlined as well as the two domains of a ($\sqrt{13} \times \sqrt{13}$) cell rotated by 33.7° relative to the 1×1. It is also better to avoid selected area diffraction, and instead use microdiffraction by creating a small probe (small spot size, smaller condenser aperture). In selected area mode it is possible for diffracted beams from an area outside the aperture to contribute to the pattern adding to the noise. Since the intensity of surface spots can vary over several orders of magnitude, a series of diffraction patterns from the same area is taken. When irradiating the area of a sample for an extended period, such as during the collection of a series of diffraction patterns, beam damage can be an issue and degrade the surface.
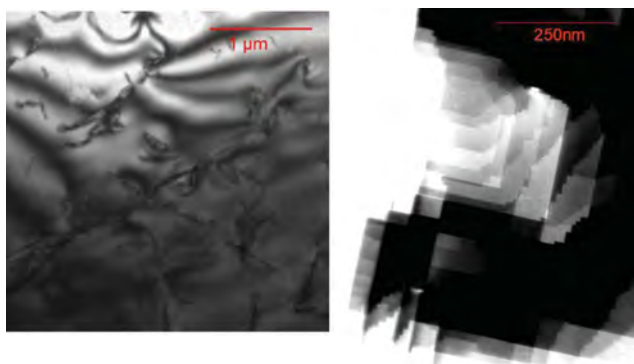
Fig. 2 (Left) Bright field TEM image taken of $SrTiO_3$ (001) sample after sample preparation. Bend contours and dislocations are present. (Right) Bright field TEM image taken of $SrTiO_3$ (001) after etching with a buffered-hydroflouric acid and annealing for 5 h at 1050 °C in flowing O_2. The ($\sqrt{13} \times \sqrt{13}$)R33.7° reconstruction is present on the surface.

Fig. 3 Off-zone TED pattern[23] of SrTiO₃ (001) after etching with buffered-hydroflouric acid and annealing for 5 h at 1050 °C in flowing O_2. Bulk 1 × 1 cell outlined in blue and two domains of the $(\sqrt{13} \times \sqrt{13})R33.7°$ reconstruction are outlined in red and yellow.

Fortunately, SrTiO₃ is robust enough that this is not a problem.

2.2 Structure determination

Diffraction patterns are then digitized to 8 bits with a 25 micron pixel size using an optical microdensitometer and a cross-correlation technique[18] is used to measure the intensities of surface spots over the series of patterns and reduce each reflection to a single intensity with its associated error calculated from standard statistical methods. The beams are then averaged over the appropriate 2D Patterson symmetry resulting in a final data set of independent reflections.

An estimate of the correct phases for the reflections is found *via* direct methods, a term used to describe a collection of structure determination techniques that exploit *a priori* information to set and enforce constraints on possible phase solutions; they cannot be completely random. One constraint is that scattering is caused by atoms, therefore the solution map should have atom-like features of high charge density, *i.e.* high scattering potential, surrounded by areas of no charge density. Another constraint is that the charge density in a real crystal is positive. Thirdly, the area of space from which the scattering originates is limited to the near-surface region. A multi-

solution technique is used to search for sets of phases that are iteratively refined based on a figure of merit. The details of direct methods and the theory behind it are described in[17,19] and references therein. The results of a direct methods analysis are represented as scattering potential maps such as the one shown in Fig. 4 for the SrTiO₃ (110) 3 × 1 reconstruction with an atomic model overlaid to illustrate the interpretation.

Structure refinement is done by assigning strontium, titanium, and oxygen atoms to high-scattering features, calculating the intensity with the chosen assignments, and comparing it to the recorded experimental intensity by a conventional R-factor or χ^2 analysis. The positions of oxygen atoms in a SrTiO₃ map are typically not found because of their weak scattering ability. In this case, knowledge of the bulk structure, the preferred coordination of the titanium and strontium, and valence compensation must be used to determine the oxygen positions.

Structure determination can prove difficult at this stage for several reasons, such as the fact that often there are multiple, different solution maps found that must be differentiated between. Moreover, since bulk reflections are removed from the diffraction data, sur-

face spots that periodically coincide with bulk spots cannot be measured. Also, unmeasured reflections and experimental error can result in a partial solution. Other unknowns that are encountered are the registry of the surface layer with the underlying bulk, as well as the out-of-plane position of atoms in a 2D map. It most certainly would be a high energy surface if atoms were constrained to the same plane and not allowed to relax and optimize bond distances.

2.3 Density functional theory

The unknowns stated above can be addressed with the help of density functional theory (DFT), a quantum mechanical approach to solving the ground state energy for a many-body system.

Over the years, the accuracy of DFT has advanced greatly and thus has become more and more integral to the structure determination process. Candidate surface structures can be modeled as a 3D periodic surface slab separated by vacuum for DFT calculations that is repeated inifinitely in all directions. There must be enough atomic layers so that the very center of the slab preserves the bulk structure and is unaffected by the surfaces. There must also be enough vacuum between slabs so that there is no interaction between them and the surface potential approaches zero in the center of the vacuum. Atom positions in the slab are optimized iteratively by DFT until atoms in the slab have moved into lower energy positions and the slab energy calculated after each iteration has converged. The final structural solution can be found by comparing the energies of different reconstructions that may have been indistinguishable with direct methods alone. DFT modeling can also act as a check for cation positions. If strong scattering atoms move away from their initial positions found with direct methods, this is a warning that the starting solution is wrong or incomplete. As shown in Fig. 4, a model of the atomic surface layer after optimizing atom positions with DFT is overlaid the initial direct methods solution. Blue atoms representing Ti atoms have moved very little in the x- and y-directions (in-plane) and still correspond well with the high scattering potential areas (white in this map).
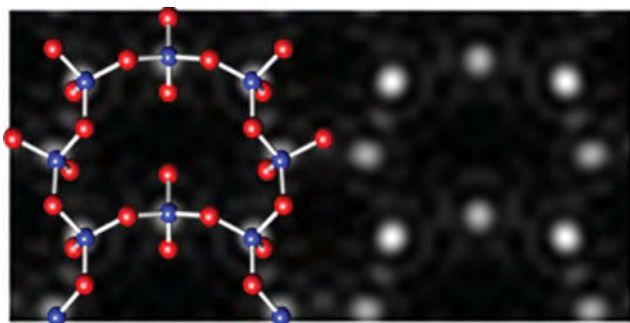
Fig. 4 Scattering potential for the $SrTiO_3$ (110) 3×1 surface structure with the surface atoms overlayed on the left half. The light features on the scattering potential map indicate areas of stronger scattering potential (*i.e.*, strong scattering species, in this case Ti). Ti in blue and oxygen in red.[25]
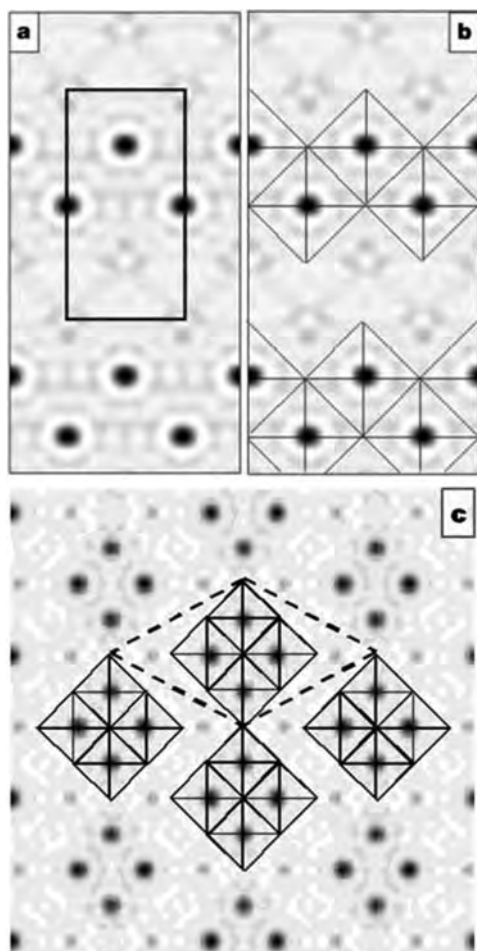
Fig. 5 a) Theoretical direct methods solution of the 2×1 structure. Scattering potential map calculated from two-dimensional code for *pm* symmetry. b) Interpretation of the map a) in terms of TiO_x units. In both cases regions of high potential—that is, possible atomic sites—are black, and subsequent analysis demonstrated that these were Ti atoms.[20] c) Scattering potential map obtained by direct methods analysis for $SrTiO_3$ (001) $c(4 \times 2)$ surface reconstruction. Dark features were determined to be Ti atom sites. Dashed line shows $c(4 \times 2)$ cell and solid lines represent TiO_x pseudo-octahedral units.[21]

3. SrTiO₃ surface structures

3.1 (001) surface: 2×1, $c(4 \times 2)$, $c(6 \times 2)$, RT13

The first $SrTiO_3$ (001) surface reconstruction to be structurally determined was the 2×1,[20] followed by the $c(4 \times 2)$,[21] $c(6 \times 2)$[22] and the RT13.[23] In all of the direct methods refinements for the $SrTiO_3$ determined reconstructions (2×1, $c(4 \times 2)$, $c(6 \times 2)$, RT13 for the (001) direction and the $n \times 1$ series for the (110) direction[16]), titanium was found to give a better fit than strontium. In Fig. 5a, the solution map for the 2×1 reconstruction, formed at 950–1050 °C under oxidizing conditions, is shown with the 2×1 repeating cell outlined and the interpretation of dark areas as Ti cations and squares representing TiO_x units. Similarly, the solution map for the $c(4 \times 2)$ reconstruction, formed at 850–930 °C under oxidizing conditions, is shown in Fig. 5c with a dashed line showing the surface unit cell. Again, the dark areas have been assigned Ti atom positions and squares are outlined showing TiO_x units. Both the 2×1 and $c(4 \times 2)$ are composed of a bulk TiO_2 layer with an additional layer of TiO_2 composition. The 2×1 is very similar to the $c(4 \times 2)$ in that a simple rearrangement of a Ti atom position is the only difference between the two structures.

The $c(6 \times 2)$ structure, formed at temperatures between 1050–1100 °C in oxidizing conditions is a more complex structure that is made up of four microscopic structurally-similar motifs with additional non-periodic TiO_2 units at the surface. The surface is a random mixture of the motifs, but each motif has short-range order. Determining the $c(6 \times 2)$ structure was very complex and required using both TED and surface X-ray diffraction to find Ti positions. Like the 2×1 and $c(4 \times 2)$, the surface is terminated with a Ti_yO_x layer. Unlike the 2×1 and $c(4 \times 2)$, the $c(6 \times 2)$ has a more than one TiO_2 unit above a bulk TiO_2 layer. It also contains both 5- and 4-fold coordinated Ti atoms, while the 2×1, $c(4 \times 2)$, and RT13 only have 5-fold coordinated Ti atoms at the surface. The most striking difference is the fact that the $c(6 \times 2)$ reconstruction is composed of multiple related, but different, structural domains, while the $c(4 \times 2)$
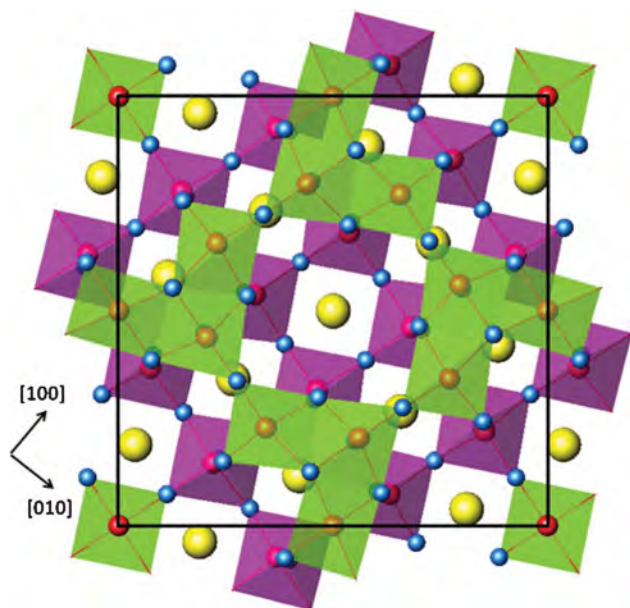
Fig. 6 Top view of SrTiO₃ (001) RT13 surface reconstruction with TiO_6 octahedra (pink) and TiO_5 polyhedra (green). Octahedra and polyhedra include a Ti atom at their center (red) and O (blue) at their corners. TiO_5 unit at corner of cell is in the subsurface. Large individual Sr atoms (yellow) are in the third layer from the surface.[23]

and 2 × 1 reconstructions are single-structure surfaces.

The RT13 reconstruction, formed at 850–1050 °C under oxidizing conditions and shown in Fig. 6, was prepared with an additional step of etching with a buffered hydrofluoric acid to preferentially remove SrO [24] before annealing, although this step may be superfluous since the RT13 has been observed without etching [25] and most likely is or becomes Ti-rich like the 2 × 1, c(4 × 2), and c(6 × 2). The RT13 structure has a ring of ten TiO_5 polyhedra units that share edges with TiO_6 octahedra located in the subsurface. There is also one TiO_5 unit in the subsurface that remains corner sharing with neighboring octahedra and is stabilized by rotations of the octahedra in the bulk beneath them. It

has a stoichiometry of 1.115 excess TiO_2 units per bulk 1 × 1 cell, slightly less than the 2 × 1 and c(4 × 2), both of which have 1.5 excess TiO_2 units per 1 × 1. Theoretically, by varying the number of Ti units in the ring, other reconstructions can be formed, such as a 3 × 3 and a $(\sqrt{5} \times \sqrt{5})R26.6°$ ("RT5"), which are indeed periodicities that have been experimentally observed. DFT has shown that these two reconstructions are energetically reasonable.

When annealing in the temperature range of 850–1050 °C, the 2 × 1, c(4 × 2), and RT13 have each been observed to form. At 850 °C, either the 2 × 1 or RT13 will form, with the RT13 being more common, while at 950 °C all three can form, with the 2 × 1 being most common. It has even been observed that

two samples annealed together can form the 2 × 1 on one sample and RT13 on the other.[25] It is apparent that the temperature is not the sole factor governing the surface structure outcome nor is annealing environment (see Table 1.) Other factors such as local variation in stoichiometry at the surface, kinetic pathways for surface diffusion, and sample preparation can also contribute.

3.2 (110) surface: n × 1 series

The n × 1 series of reconstructions for the (110) direction of SrTiO₃ include the observed 3 × 1, 4 × 1, 5 × 1, and 6 × 1 periodicities.[16] TED data from the 3 × 1 reconstruction (Fig. 4) was used to determine its structure, which is comprised of corner-sharing TiO_4 tetrahedra, arranged into six-and eight-member rings. By varying the number of TiO_4 units in the larger ring, reconstructions with 2 × 1, 4 × 1, 5 × 1, 6 × 1, *etc.* can be formed, thus creating a homologous series shown in Fig. 7, and confirmed with DFT and scanning tunneling microscopy. As n increases, the TiO_2 surface excess decreases.

4. Discussion

The emerging theme of the discussed reconstructions is that the surface can be considered as a network of corner- or edge-sharing TiO_x units in varying stoichiometries. The network can range from ordered to pseudo-ordered, like the c(6 × 2), to a disordered glass-like surface layer made up of TiO_x units. The (110) n × 1 series and the theoretical investigation of the (001) 3 × 3 and RT5 adapted from the RT13 demonstrate the high level of structural similarity between the reconstructions. In all cases, there are additional surface Ti atoms that are
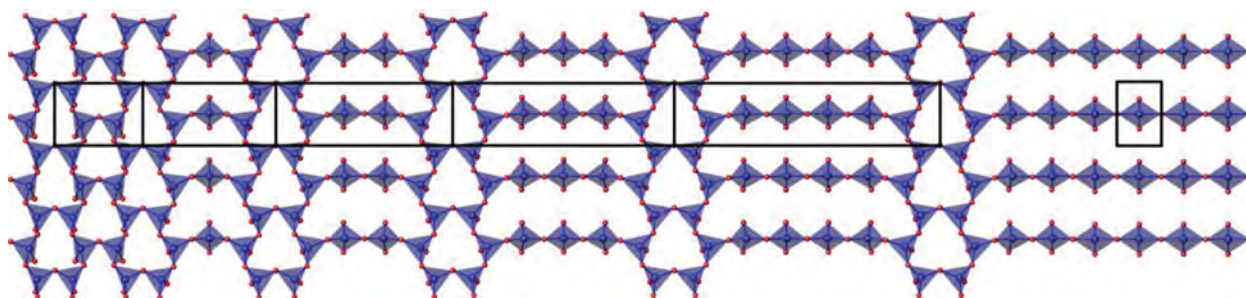
Fig. 7 SrTiO₃ (110) surface structures of the homologous series of n × 1 surface structures viewed perpendicular to the surface. For clarity, the bulk is omitted. TiO_4 tetrahedra are shown in blue, with oxide anions in red. Unit cells are outlined in black, from left to right n = 2,3,4,5,6,∞.[16]

under-coordinated relative to bulk Ti which are octahedrally coordinated to six oxygen atoms. The under-coordination of Ti results in slightly shorter Ti-O bond lengths and more covalent bonds.

In some TED patterns, the observed surface reconstruction spots will appear as streaks rather than resolved dots if there is some periodic disorder in the surface. Often, this means the structure is not fully formed and upon further annealing, the reconstruction will fully order itself, resulting in clearly defined spots in the diffraction pattern. Under oxidizing conditions, it can be expected that the surface will exist in varying states of disordered TiO_x units and, when annealed, the local stoichiometry and kinetics (as well as sample preparation details) will dictate what reconstruction is formed.

As of yet, it has not been determined why a 2×1 might form rather than $c(4 \times 2)$ considering they have the same surface stoichiometry. However, the conclusions drawn from examining the $SrTiO_3$ surface reconstructions that have been determined as of now as a whole are quite powerful. Applying this knowledge to solving other $SrTiO_3$ surface reconstructions will most certainly simplify and speed up the process with the ultimate goal to relate what we know about $SrTiO_3$ surfaces to other oxide materials.

References

1 T. Ishibashi, T. Kawahara, H. Kaneko and K. Sato, *IEEE Trans. Appl. Supercond.*, 1999, **9**, 2383–2386.

2 Q. D. Jiang and J. Zegenhagen, *Surf. Sci.*, 1995, **338**, L882–L888.

3 J. Zegenhagen, T. Haage and Q. D. Jiang, *Appl. Phys. A: Mater. Sci. Process.*, 1998, **67**, 711–722.

4 M. Kawasaki, *Appl. Surf. Sci.*, 1996, **107**, 102–106.

5 T. Ohnishi, K. Shibuya, M. Lippmaa, D. Kobayashi, H. Kumigashira, M. Oshima and H. Koinuma, *Appl. Phys. Lett.*, 2004, **85**, 272–274.

6 R. Droopad, Z. Yu, J. Ramdani, L. Hilt, J. Curless, C. Overgaard, J. L. Edwards, J. Finder, K. Eisenbeiser and W. Ooms, *Mater. Sci. Eng., B*, 2001, **87**, 292–296.

7 K. Eisenbeiser, R. Emrick, R. Droopad, Z. Yu, J. Finder, S. Rockwell, J. Holmes, C. Overgaard and W. Ooms, *IEEE Electron Device Lett.*, 2006, **23**, 300–302.

8 R. A. McKee, F. J. Walker and M. F. Chisholm, *Phys. Rev. Lett.*, 1998, **81**, 3014–3017.

9 R. K. Sharma, A. Kumar and J. M. Anthony, *JOM*, 2001, **53**, 53–55.

10 Y. Liang and D. A. Bonnell, *Surf. Sci.*, 1993, **285**, L510–L516.

11 R. Martin, *Surf. Sci.*, 2002, **516**, 33–42.

12 A. F. Santander-Syro, O. Copie, T. Kondo, F. Fortuna, S. Pailhes, R. Weht, X. G. Qiu, F. Bertran, A. Nicolaou, A. Taleb-Ibrahimi, P. Le Fevre, G. Herranz, M. Bibes, N. Reyren, Y. Apertet, P. Lecoeur, A. Barthelemy and M. J. Rozenberg, *Nature*, 2011, **469**, 189–193.

13 G. Singh-Bhalla, C. Bell, J. Ravichandran, W. Siemons, Y. Hikita, S. Salahuddin, A. F. Hebard, H. Y. Hwang and R. Ramesh, *Nat. Phys.*, 2011, **7**, 80–86.

14 A. N. Chiaramonti, C. H. Lanier, L. D. Marks and P. C. Stair, *Surf. Sci.*, 2008, **602**, 3018–3025.

15 B. C. Russell and M. R. Castell, *Phys. Rev. B: Condens. Matter Mater. Phys.*, 2008, **77**, 245414.

16 J. A. Enterkin, A. K. Subramanian, B. C. Russell, M. R. Castell, K. R. Poeppelmeier and L. D. Marks, *Nat Mater*, 2010, **9**, 245–248.

17 L. D. Marks, W. Sinkler and E. Landree, *Acta Crystallogr., Sect. A: Found. Crystallogr.*, 1999, **55**, 601–612.

18 P. Xu, G. Jayaram and L. D. Marks, *Ultramicroscopy*, 1994, **53**, 15–18.

19 P. Xu, D. Dunn, J. P. Zhang and L. D. Marks, *Surface Science Letters*, 1993, **285**, L479–L485.

20 N. Erdman, K. R. Poeppelmeier, M. Asta, O. Warschkow, D. E. Ellis and L. D. Marks, *Nature*, 2002, **419**, 55–58.

21 N. Erdman, O. Warschkow, M. Asta, K. R. Poeppelmeier, D. E. Ellis and L. D. Marks, *J. Am. Chem. Soc.*, 2003, **125**, 10050–10056.

22 C. H. Lanier, A. van de Walle, N. Erdman, E. Landree, O. Warschkow, A. Kazimirov, K. R. Poeppelmeier, J. Zegenhagen, M. Asta and L. D. Marks, *arXiv:0707.2561*, 2007.

23 D. M. Kienzle, A. E. Becerra-Toledo and L. D. Marks, *Phys. Rev. Lett.*, 2011, **106**, 176102–176102.

24 M. Lippmaa, K. Takahashi, S. Ohashi, N. Nakagawa, T. Sato, M. Iwatsuki, H. Koinuma and M. Kawasaki, *Ferroelectrics*, 1999, **224**, 373–378.

25 J. A. Enterkin, *A Chemical Approach to Understanding Oxide Surface Structure and Reactivity*, 2010.

26 B. Cord and R. Courths, *Surf. Sci.*, 1985, **162**, 34–38.

27 G. Charlton, S. Brennan, C. A. Muryn, R. McGrath, D. Norman, T. S. Turner and G. Thornton, *Surf. Sci.*, 2000, **457**, L376–L380.

28 V. Henrich, G. Dresselhaus and H. Zeiger, *Phys. Rev. B*, 1978, **17**, 4908–4921.

29 P. A. W. van der Heide, Q. D. Jiang, Y. S. Kim and J. W. Rabalais, *Surf. Sci.*, 2001, **473**, 59–70.

30 J. E. T. Andersen and P. J. Mo\ller, *Appl. Phys. Lett.*, 1990, **56**, 1847–1847.

31 M. Naito and H. Sato, *Phys. C*, 1994, **229**, 1–11.

32 R. Martin, *Surf. Sci.*, 2002, **505**, 1–13.

33 S.-h. Phark, Y. J. Chang and T. Won Noh, *Appl. Phys. Lett.*, 2011, **98**, 161908–161908.

34 T. Matsumoto, H. Tanaka, T. Kawai and S. Kawai, *Surface Science Letters*, 1992, **278**, L153–L158.

35 T. Kubo and H. Nozoye, *Surf. Sci.*, 2003, **542**, 177–191.

36 Q. D. Jiang and J. Zegenhagen, *Surf. Sci.*, 1999, **425**, 343–354.

37 Q. Jiang and J. Zegenhagen, *Surf. Sci.*, 1996, **367**, L42–L46.

38 H. Tanaka, T. Matsumoto, T. Kawai and S. Kawai, *Jpn. J. Appl. Phys.*, 1993, **32**, 1405–1409.

39 T. Kubo and H. Nozoye, *Phys. Rev. Lett.*, 2001, **86**, 1801–1804.

40 R. Akiyama, T. Matsumoto, H. Tanaka and T. Kawai, *Jpn. J. Appl. Phys.*, 1997, **36**, 3881–3886.

41 M. S. Martn Gonzalez, M. H. Aguirre, E. Moran, M. A. Alario-Franco, V. Perez-Dieste, J. Avila and M. C. Asensio, *Solid State Sci.*, 2000, **2**, 519–524.